



OPEN ACCESS

EDITED BY

Rumao Tao,
China Academy of Engineering Physics,
China

REVIEWED BY

Hongfei Jiao,
Tongji University, China
Yuxuan Ren,
Fudan University, China
Shijun Zhu,
Nanjing University of Science and
Technology, China

*CORRESPONDENCE

Lei Huang,
✉ hl@tsinghua.edu.cn

RECEIVED 23 March 2023

ACCEPTED 03 May 2023

PUBLISHED 23 May 2023

CITATION

Lin S, Wang D, Zheng Y, Guo L, Zhang Y,
Zhuang Y and Huang L (2023), Helicity
and topological charge tunable optical
vortex based on a Hermite-Gaussian
beam dynamically controlled folded-
cavity resonator.
Front. Phys. 11:1192257.
doi: 10.3389/fphy.2023.1192257

COPYRIGHT

© 2023 Lin, Wang, Zheng, Guo, Zhang,
Zhuang and Huang. This is an open-
access article distributed under the terms
of the [Creative Commons Attribution
License \(CC BY\)](https://creativecommons.org/licenses/by/4.0/). The use, distribution or
reproduction in other forums is
permitted, provided the original author(s)
and the copyright owner(s) are credited
and that the original publication in this
journal is cited, in accordance with
accepted academic practice. No use,
distribution or reproduction is permitted
which does not comply with these terms.

Helicity and topological charge tunable optical vortex based on a Hermite-Gaussian beam dynamically controlled folded-cavity resonator

Shibing Lin^{1,2}, Deen Wang^{1,2}, Yamin Zheng^{1,2}, Liquan Guo^{1,2},
Yifan Zhang^{1,2}, Yongchen Zhuang^{1,2} and Lei Huang^{1,2*}

¹Key Laboratory of Photonic Control Technology (Tsinghua University), Ministry of Education, Beijing, China, ²Department of Precision Instrument, Tsinghua University, Beijing, China

Helicity and topological charge are two important characteristic parameters for vortex beam applications, including optical communications, optical manipulation and material processing, etc. In this work, a helicity and topological charge tunable optical vortex laser based on a folded resonant cavity is presented. In the resonant cavity, a Z-shaped structure is adopted and two deformable mirrors (DMs) are cascaded into the cavity as intro-cavity modulation elements. By applying different voltage combinations to the DMs, the Hermite-Gaussian (HG) beam with different indices and distribution orientations θ could be generated from the Z-shaped folded-cavity resonator. An extra-cavity astigmatic mode converter is adopted to convert the generated HG beam to the corresponding vortex beam with tunable helicity and topological charge, and the simulation results verified the feasibility of the presented vortex laser. In the experiment, the $HG_{m,0}^{\theta}$ beam ($m = 1$ to 10 and $\theta = -90^{\circ}$ to 90°) and the vortex beam (topological charge l from ± 1 to ± 10 and left/right helicity) were flexibly achieved by simply adjusting the driving voltage combinations of the intra-cavity cascaded DMs.

KEYWORDS

helicity, topological charge, vortex beam, deformable mirror, Hermite-Gaussian

1 Introduction

Vortex beam with the helical phase in the form of $\exp(il\theta)$ has wide application in many fields. Two principal parameters, the topological charge (TC: l) and the helicity (the sign of l), are important to the application of vortex beam as they could effectively expand the type of vortex beam. In the optical communications field [1], more types of vortex beams could enhance communication capacity and security. In the optical manipulation field, the vortex beam with tunable TC and helicity could provide more operational diversity [2]. In the material processing field, the nanostructure with different chirality structures could be realized by using the TC and helicity tunable vortex beam [3].

The generation of the helicity and TC tunable vortex beam has been widely studied and various methods have been reported [4–15]. One of the most direct methods is to generate a helicity and TC tunable vortex beam from a resonant cavity with intra-cavity modulation. By introducing helicity and TC selection elements into a resonant cavity, such as two nanowires [4], a YAG crystal [5], a quarter-wave plate [6], a black phosphorus plate [7], etc., the vortex

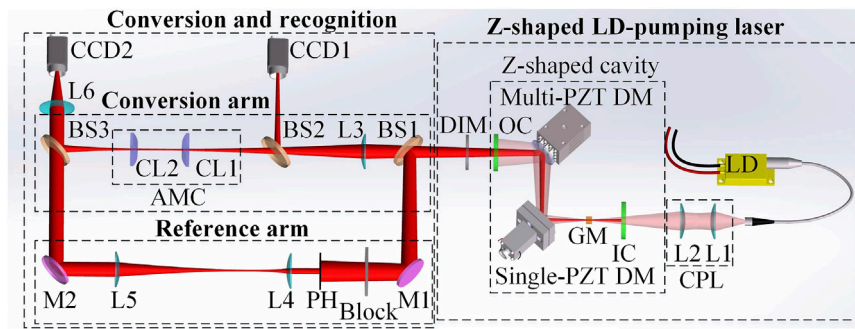


FIGURE 1
Schematic diagram of the TC and helicity tunable vortex laser.

beam with controllable helicity (left/right) and the TC (up to ± 2) could be generated. In addition, by adjusting the intra-cavity crystal [8] or the output coupler lens [9] to specific angles, the vortex beam with determined helicity and TC of 1 was obtained. These methods mentioned above could flexibly generate a vortex beam with controllable TC and helicity by intra-cavity modulation but the TC is usually limited within ± 2 .

Apart from the mentioned methods obtaining the target vortex beam directly with intra-cavity modulation, the extra-cavity conversion based on the Hermite-Gaussian (HG) beam could also be used to generate the TC and helicity tunable vortex beam. The conversion elements, such as spiral phase plate (SPP) [10–12], spatial light modulation (SLM) [13–15] and digital micromirror device (DMD) [16, 17], could convert a fundamental mode beam to the vortex beam with target TCs and helicity. However, the SPP is customized and a SPP could only convert the fundamental mode HG beam to one type of vortex beam. Thus, a large amount of customized SPPs is needed to achieve different kinds of TC and helicity. For the SLM/DMD conversion, the vortex beam with target TCs and helicity could be realized by loading special computer-generated holograms. However, the energy loss of these diffractive optical elements is inevitable in the conversion process, which limits their application in the high-power laser field. Besides the mentioned elements, the extra-cavity astigmatic mode converter (AMC) could convert a $HG_{m,n}$ beam to a $LG_{p,l}$ beam with negligible energy loss. The relationship of the indices has been revealed in [18, 19] and satisfies the equations of $p = \min\{m,n\}$, $l = m-n$. By the AMC conversion, Wang et al [20] obtained the $HG_{m,0}$ beam by intra-cavity mirror curvature dynamically control method, and the TC tunable vortex beam with single helicity is achieved based on AMC conversion. Shen et al [21] realized the rotation from $HG_{m,0}$ to $HG_{0,n}$ beam by dual off-axis pumping, while the TC and helicity tunable vortex beam is further generated by AMC conversion. However, the off-axis adjustment is lack of flexibility as it is accomplished based on complex and inflexible mechanical adjustment.

In this paper, a vortex laser that could flexibly generate the TC and helicity tunable vortex beam is reported. In the presented vortex laser, two cascaded deformable mirrors (DM), a single-piezoelectric (PZT) DM and a multi-PZT DM, are set as the intra-cavity modulation elements in a Z-shaped folded resonant cavity.

Through loading different driving voltage combinations to the DMs, different surface shapes are generated and the intra-cavity mode is modulated. Thus, the HG beam in the form of $HG_{m,0}$ with different indices and distribution orientations is generated. After that, the HG beam is converted by an extra-cavity AMC, realizing vortex beam with helicity and TC tunability. In the experiment, the TC (± 1 to ± 10) and helicity (left or right) of the vortex beam could be flexibly controlled by loading suitable driving voltage combinations to the DMs.

2 Methods

Figure 1 shows the schematic diagram of the proposed vortex laser, which mainly contains a Z-shaped LD-pumping laser and a conversion and recognition module. In the Z-shaped LD-pumping laser, the pumping beam emitted from a fiber-coupled LD (20W, 976nm, 0.22NA/105 μm core diameter, BWT Beijing LTD.) is focused into a gain medium GM (Yb: CALGO, 5 a. t.%, a-cut, 2 mm \times 2 mm \times 4mm, AR@1064 nm) with the beam waist radius of 200 μm . The coupling lens CPL is composed of lenses L1 and L2 (30 mm and 60 mm focus lengths). The Z-shaped cavity consists of a plane input-coupler IC (HR@1064nm, AR@976 nm), a single-PZT DM (\varnothing 50 mm, HR@1064 nm/45°), a multi-PZT DM (\varnothing 25 mm, HR@1064 nm/45°) and a concave output-coupler OC (100 mm curvature radius, 2%T@1064 nm, HR@976 nm). To avoid the influence of the pumping beam in the subsequent optical route, a dichroic mirror DIM (AR@1064 nm, HR@976 nm) is adopted after the OC to filter the pumping beam of 976 nm.

In the conversion and recognition module, the incident HG beam is converted to the corresponding LG beam in the conversion arm, while a reference beam used to recognize the converted LG beam is obtained in the reference arm. The conversion arm is composed of three beam splitters (BS1: transmittance and reflectance ratio TRR of 1:9@1064nm, BS2 and BS3: TRR of 1:1@1064 nm), a matching lens L3 (175 mm focal length), and an AMC (two identical cylindrical lenses CL1 and CL2, both 25 mm in focal length). The BS1 splits part of the HG beam generated from the Z-shaped laser into the reference arm as an input. L3 focuses the incident HG beam into the AMC to satisfy the AMC conversion condition [18]. The BS2 splits part of the HG beam into CCD1

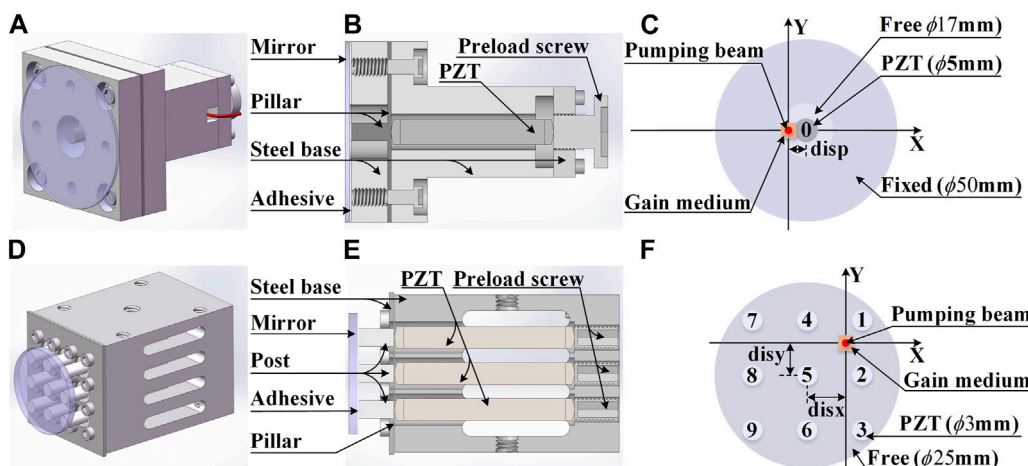


FIGURE 2 Outside views (A, D), section views (B, E) and constraints of the mirrors (C, F) of two cascaded DMs.

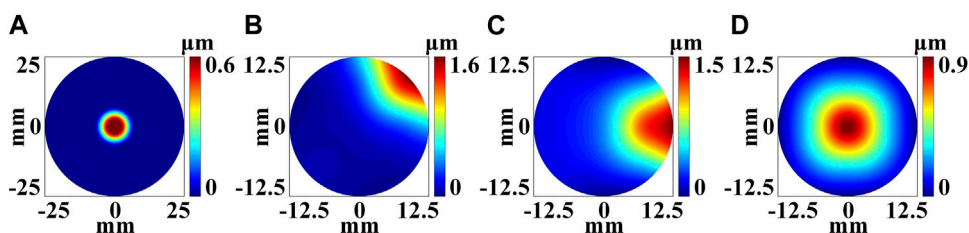


FIGURE 3 Surface shapes of two cascaded DMs with 10 V driving voltage of typical PZTs. PZT 0 (A) of the single-PZT DM. PZT 1 (B), 2 (C) and 5 (D) of the multi-PZT DM.

(Point Grey, GS3-U3-14S5M) and the corresponding intensity pattern is recorded. After the AMC conversion, the converted LG beam is reflected by BS3 and focused by L6 (30 mm focal length) into CCD2 (Point Grey, GS3-U3-14S5M). Note that the intensity pattern of the converted LG beam will be recorded by CCD2 when only the LG beam incident into CCD2. The reference arm consists of two reflection mirrors (M1 and M2: HR@1064 nm/45°), a switch block, a pinhole PH (2 mm-diameter hole), and a telescope system (L4 and L5, focal length of 25mm and 125 mm). The block has two states of “on/off” and determines whether the HG beam is allowed to enter into the reference arm. Lenses L4 and L5 are set non-confocal. When the block is in the state of “on,” a spherical reference beam will be generated based on the small central part of the incident beam that passes through the PH. The interference fringe of the spherical reference beam and the vortex beam is recorded by CCD2. Thus, the helicity and TC of the vortex beam will be recognized.

Two cascaded DMs, including a single-PZT DM and a multi-PZT DM, are adopted in the vortex laser. Figure 2 shows the outside views, section views and constraints of the two DM mirrors. From Figure 2B, it could be seen that the single-PZT DM consists of a mirror, a pillar, a steel base, an adhesive, a PZT and a preload screw. The multi-PZT DM [shown in Figure 2E] shares the same basic structure of the single-PZT DM, except that it contains an additional

post and has 9 PZTs. The distances between two adjacent PZTs along X and Y-axes are both 8 mm in the multi-PZT DM. Figures 2C, F show the mirror constraints of the DMs, which could be divided into assembly constraints and structural constraints. The assembly constraints [disp, disx and disy in Figures 2C, F] represent the location relationship among the pumping beam, the gain medium and the center of the mirror. The constraints of mirror structure shown in Figures 2C, F contain the fixed area, the PZT area and the free area. It should be noted that the numbers 0–9 in Figures 2C, F represents the corresponding PZT. The simulation models of the DMs are built [22]. Figure 3 shows the simulation results of the surface shapes of the two cascaded DMs with 10 V driving voltage of typical PZTs, including PZT 0 of the single-PZT DM, PZTs 1, 2 and 5 of the multi-PZT DM. The simulated influence functions (IF, surface shape with PZT driving voltage of 1 V) of PZT 0–9 could be calculated. Thus, the surface shapes $S(x, y)$ of the cascaded DMs could be expressed as Eq. 1 and be controlled by applying different driving voltage combinations [Eq. 2].

$$S_j(x, y) = \sum_i^{N_j} V_i \cdot IF_i(x, y), j = 1, 2 \tag{1}$$

$$V = [V_0] + [V_k]_{k=1-9} \tag{2}$$

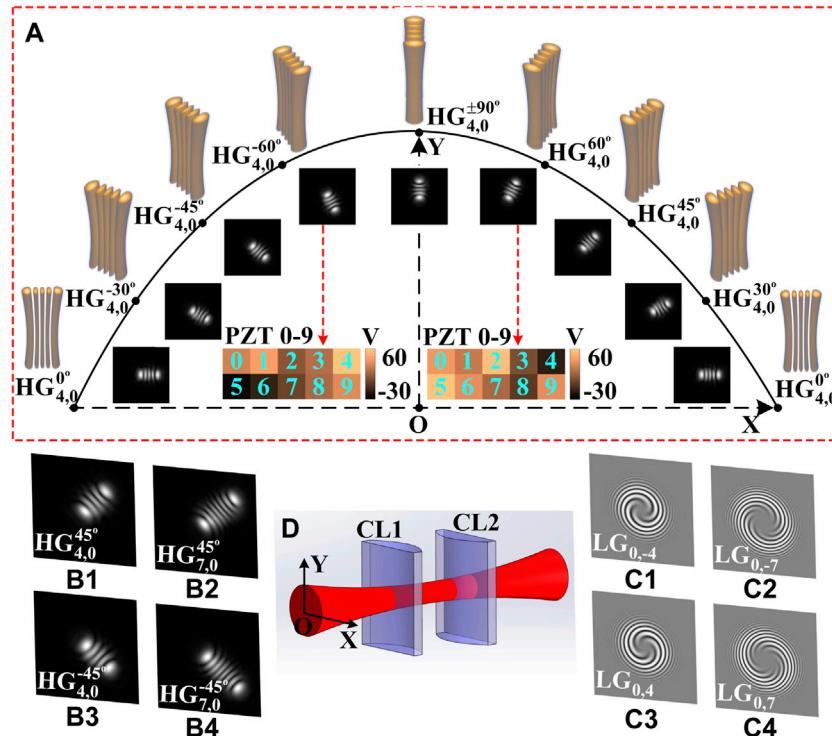


FIGURE 4 Simulation results of the TC and helicity tunable vortex laser. (A) 3D beam propagation and intensity patterns of $HG_{4,0}^{\theta}$ beams, and driving voltage combinations for $HG_{4,0}^{\pm 45^{\circ}}$ beams. (B1–B4) Intensity patterns of $HG_{4,0}^{\pm 45^{\circ}}$ and $HG_{7,0}^{\pm 45^{\circ}}$ beams. (C1–C4) Interference fringes of the spherical reference beam and vortex beams converted from the HG beams in (B1–B4) through the AMC (D), respectively.

where j represents the single/multi-PZT DM. N_j represents the total number of the PZTs. V_i and $IF_i(x, y)$ represent the driving voltage and influence function of the i^{th} PZT, respectively.

In the Z-shaped resonant cavity, the surface shape distributions of DMs could be adjusted by loading different PZT voltages according to Eq. 1, and the surface shape distributions of DMs will introduce an additional phase into the intra-cavity propagation light field to realize intra-cavity modulation [23]. Due to the Single/Multi-PZT DMs are cascaded and various intra-cavity modulation conditions could be produced by adjusting PZT voltages, when the intra-cavity modulation of a tilt HG mode is satisfied, a tilt HG mode could be generated and the rotation of HG beam is realized. Thus, a mode-tunable $HG_{m,0}$ beam with different distribution orientations could be generated from the cavity when suitable driving voltage combinations are applied to the cascaded DMs. The distribution orientation could be expressed as θ (positive of clockwise rotation), which represents the angle between the intensity distribution direction of the HG beam and the X-axis (Figure 4). After passing through the extra-cavity AMC, the HG beam is converted to the corresponding LG beam when the distribution orientation of the HG beam satisfies the conversion condition. Eventually, the opposite helicity vortex beam could be achieved from the conversion of the HG beam of $\theta = \pm 45^{\circ}$. Therefore, the TC l and the helicity (the sign of l , left or right) of the vortex beam could be flexibly tuned by applying different driving voltage combinations to the cascaded DMs.

3 Results and discussion

3.1 Simulation results

To verify the feasibility of the proposed vortex laser, a numerical simulation is carried out based on the mode modulation regulation of the vortex beam [23]. In the simulation, structure parameters of the Z-shape cavity (Figure 1) are set as follows: the distance between IC and the right surface of the GM is 6mm; the distance between the left surface of the GM and the single-PZT DM is 46mm; the distance between the cascaded DMs is 30 mm; the distance between the multi-PZT DM and OC is 25 mm; the assembly constraints (disp, disx and disy) of the DMs are 3.5 mm, 0 mm and 3 mm. $HG_{m,0}$ beams with distribution orientation θ is expressed as $HG_{m,0}^{\theta}$. Typical simulation results of the generated HG beam and the vortex beam are shown in Figure 4, in which $HG_{4,0}^{\theta}$ beams are selected as the example. From the 3D beam propagation and intensity patterns shown in Figure 4A, it could be seen that the distribution orientation θ could be widely and flexibly tuned from -90° to 90° . Driving voltage combinations for the $HG_{4,0}^{\pm 45^{\circ}}$ beams are also displayed in Figure 4A. For the HG beams with different distribution orientations or different TCs, corresponding driving voltage combinations need to be applied to the cascaded DMs; Figures 4B1–B4 are the intensity patterns of the generated $HG_{4,0}$ and $HG_{7,0}$ beams with distribution orientation θ of $\pm 45^{\circ}$; Figures 4C1–C4 show the interference fringes of the spherical reference beam and the LG beams converted from the HG beams shown in Figures 4B1–B4,

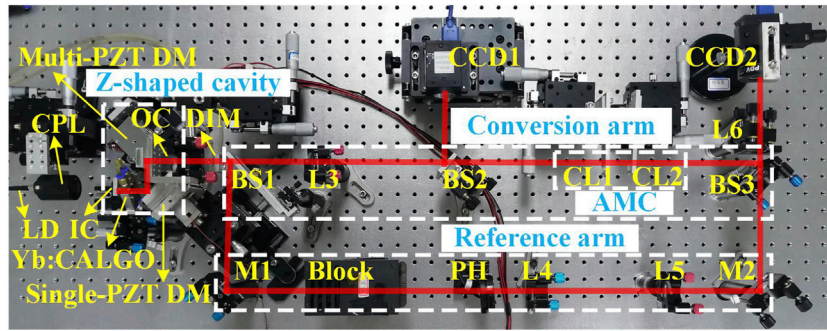


FIGURE 5 Experimental setup of the TC and helicity tunable vortex laser.

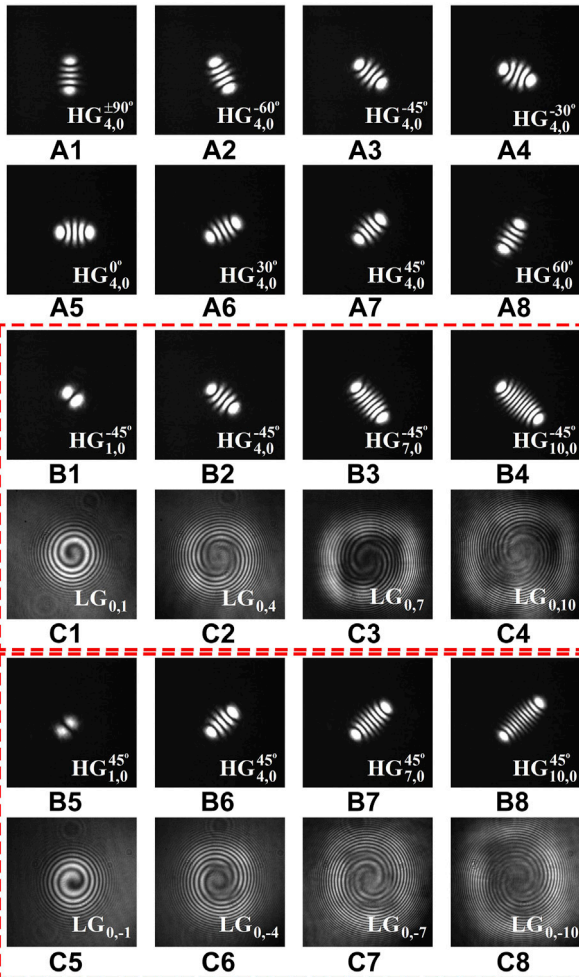


FIGURE 6 Experiment results of the TC and helicity tunable vortex laser. (A1–A8) $HG_{4,0}^{\theta}$ beams with $\theta = +90^{\circ}, +60^{\circ}, +45^{\circ}, +30^{\circ}$ and 0° . (B1–B8) Four types of HG beams ($HG_{1,0}^{\pm 45^{\circ}}, HG_{4,0}^{\pm 45^{\circ}}, HG_{7,0}^{\pm 45^{\circ}}$ and $HG_{10,0}^{\pm 45^{\circ}}$). (C1)–(C8) Interference fringes of the spherical reference beam and the LG beams converted from the HG beams in (B1–B8), respectively.

TABLE 1 Driving voltage combinations corresponding to the experiment results in Figure 6.

Mode	V_0/V	V_{1-9}/V	Mode	V_0/V	V_{1-9}/V
$HG_{4,0}^{+90^{\circ}}$	[−20]	$\begin{bmatrix} 41 & 7 & 1 \\ 86 & 67 & 82 \\ 37 & -7 & -7 \end{bmatrix}$	$HG_{4,0}^{60^{\circ}}$	[40]	$\begin{bmatrix} 40 & 57 & 48 \\ 112 & -60 & -59 \\ 20 & 101 & 72 \end{bmatrix}$
$HG_{4,0}^{-60^{\circ}}$	[48]	$\begin{bmatrix} 2 & 31 & -21 \\ 66 & 28 & 30 \\ -14 & 35 & -8 \end{bmatrix}$	$HG_{1,0}^{-45^{\circ}}$	[20]	$\begin{bmatrix} 82 & 18 & 36 \\ -26 & 29 & -25 \\ -5 & 74 & 80 \end{bmatrix}$
$HG_{4,0}^{-45^{\circ}}$	[22]	$\begin{bmatrix} 0 & 2 & 52 \\ 24 & 28 & 63 \\ 43 & 41 & 31 \end{bmatrix}$	$HG_{1,0}^{45^{\circ}}$	[−52]	$\begin{bmatrix} 37 & -41 & -17 \\ -52 & -60 & -51 \\ -60 & 87 & 51 \end{bmatrix}$
$HG_{4,0}^{-30^{\circ}}$	[−2]	$\begin{bmatrix} -24 & -3 & -60 \\ -60 & -30 & -32 \\ -57 & 65 & 79 \end{bmatrix}$	$HG_{7,0}^{-45^{\circ}}$	[−30]	$\begin{bmatrix} -33 & 80 & -43 \\ 14 & 54 & -58 \\ 11 & 1 & -2 \end{bmatrix}$
$HG_{4,0}^{0^{\circ}}$	[−35]	$\begin{bmatrix} 30 & 65 & -53 \\ 32 & 90 & 46 \\ 25 & 79 & 94 \end{bmatrix}$	$HG_{7,0}^{45^{\circ}}$	[−60]	$\begin{bmatrix} 16 & 82 & -60 \\ 21 & -25 & 37 \\ -60 & -60 & -60 \end{bmatrix}$
$HG_{4,0}^{30^{\circ}}$	[10]	$\begin{bmatrix} 23 & 80 & -42 \\ -42 & -58 & 90 \\ 8 & -18 & 19 \end{bmatrix}$	$HG_{10,0}^{-45^{\circ}}$	[−40]	$\begin{bmatrix} -59 & -30 & 63 \\ -30 & 90 & 105 \\ 98 & -51 & 84 \end{bmatrix}$
$HG_{4,0}^{45^{\circ}}$	[−9]	$\begin{bmatrix} 102 & 96 & 84 \\ 29 & 116 & 80 \\ -42 & 96 & -59 \end{bmatrix}$	$HG_{10,0}^{45^{\circ}}$	[0]	$\begin{bmatrix} 115 & 30 & 67 \\ 20 & -60 & 119 \\ -9 & 65 & 111 \end{bmatrix}$

respectively. It could be seen that the TC ($\pm 4, \pm 7$) and helicity (left or right) of the generated vortex beam are both tunable by flexibly loading the driving voltage combinations. The maximum order m and the precision of θ are numerically investigated and equal to 14 and 5° , respectively. In experiment, the precision of θ could be further improved due to the voltage precision of 0.01V, which is more precise than the simulation setting.

3.2 Experiment results

Figure 5 shows the experimental setup of the TC and helicity tunable vortex laser. In the experiment, all the parameters of the

Z-shaped LD-pumping laser are the same as the simulation. Before loading driving voltages to the DMs, the Z-shaped LD-pumping laser is first precisely adjusted to obtain the fundamental mode at the pumping current of 1.3 A (maximum current of the LD is 7.5 A in our setup). Figure 6 displays the experiment results. In the experiment, the distribution orientation θ can be continuously tuned from -90° to 90° by loading different driving voltage combinations. As the examples; Figures 6A1–A8 show the intensity patterns of the generated $HG_{4,0}^{\pm 90^\circ}$, $HG_{4,0}^{\pm 60^\circ}$, $HG_{4,0}^{\pm 45^\circ}$, $HG_{4,0}^{\pm 30^\circ}$ and $HG_{4,0}^{0^\circ}$ beams recorded by CCD1. In addition, the mode of the HG beam with a certain distribution orientation θ is also adjustable (from $m = 1$ – 10) in the experiment. Figures 6B1–B8 show the experiment results of four types of HG beams with the same helicity ($HG_{1,0}^{\pm 45^\circ}$, $HG_{4,0}^{\pm 45^\circ}$, $HG_{7,0}^{\pm 45^\circ}$ and $HG_{10,0}^{\pm 45^\circ}$). It should be noted that the TC of the generated vortex beam can be flexibly tuned from ± 1 to ± 10 by loading driving voltage combinations in the experiment. Limited by the length of the paper, other types of vortex beams are not listed in Figure 6; Figures 6C1–C8 present the interference fringes of the spherical reference beam and the LG beams converted from the HG beams shown in Figures 6B1–B8, respectively. The helicity (the signs of l) in Figures 6C1–6C4 are the same (right) and opposite to that (left) in Figures 6C5–C8. This indicates that the helicity (left or right) of the vortex beam is controllable in the experiment setup by loading different driving voltage combinations. The driving voltage combinations corresponding to the experiment results in Figure 6 are listed in Table 1. In the experiment, the initial driving voltage combination is set based on the simulation results. According to the intensity pattern recorded by CCD1, the driving voltage combination will be adjusted in several iterations to generate the target beam. Noted that the voltage difference between two adjacent PZTs should be controlled lower than 200 V to avoid damaging the DM during the iterations. It is worthy to mention that in the practical vortex laser, operators can make a look-up-table before use. When operation, the target vortex beam with specific TC and helicity can be efficiently achieved by loading the related driving voltage combinations in the look-up-table.

According to the simulation and experiment results, the HG beam could be rotated from -90° to 90° in the vortex laser, which reduces the assembly requirements of the orientation of the AMC to convert the HG beam to the LG beam. Two kinds of HG beams with orthogonal distribution orientations could always be achieved by selecting suitable driving voltage combinations to generate helicity and topological charge tunable vortex beams based on AMC conversion. The distribution directions of HG beams could be expressed by $\tan(\theta)$, where θ represents the distribution orientations of HG beams. For a θ exceeds the range from -90° to 90° , the distribution direction will be identical to a corresponding distribution orientation in the range from -90° to 90° according to the tangent function. Thus, the distribution orientations of θ outside the range are not been considered in this work.

The method could avoid the complex mechanical off-axis adjustment in [15] and could flexibly generate the TC and helicity tunable vortex beam by loading suitable driving voltage combination of DMs. Most importantly, higher order topological charge is possible by optimizing the driving voltage combinations. Note that a complex multiple-PZT DM could realize the function of the cascaded DMs in this work, but the requirements of the multiple-PZT DM will be more complex and the cost will

increase. The cascaded DMs adopted here could shape the laser modes with decreased requirement and cost.

4 Conclusion

In conclusion, a TC and helicity tunable vortex laser based on a Z-shaped resonant cavity and an extra-cavity AMC, is proposed. This laser adopts two cascaded DMs, a single-PZT DM and a multi-PZT DM, as the intra-cavity modulation elements in the Z-shaped resonant cavity. The HG beam in the form of $HG_{m,0}^\theta$ with tunable index m and θ is generated by applying suitable driving voltage combinations to the cascaded DMs. Converted by the AMC, the HG beam is transformed to the corresponding vortex beam. Simulation is carried out and the tunability of the TC and helicity is investigated. Experiment results show that by loading different driving voltage combinations, the mode (1 – 10) and distribution orientation (-90° to 90°) of the HG beam can be continuously adjusted, and consequently the TC (± 1 to ± 10) and the helicity (left or right) of the converted vortex beam is flexibly tuned.

Data availability statement

The original contributions presented in the study are included in the article/supplementary material, further inquiries can be directed to the corresponding author.

Author contributions

SL and LH contributed to conception and design of the study. SL performed the simulation and the experiment. SL, LH, DW, YZ, LG, YFZ, and YGZ contributed to writing and editing the manuscript. All authors contributed to the article and approved the submitted version.

Funding

This work was supported by the National Natural Science Foundation of China (No. 61775112).

Conflict of interest

The authors declare that the research was conducted in the absence of any commercial or financial relationships that could be construed as a potential conflict of interest.

Publisher's note

All claims expressed in this article are solely those of the authors and do not necessarily represent those of their affiliated organizations, or those of the publisher, the editors and the reviewers. Any product that may be evaluated in this article, or claim that may be made by its manufacturer, is not guaranteed or endorsed by the publisher.

References

- Wang J. Advances in communications using optical vortices. *Photon Res* (2016) 4: B14–B28. doi:10.1364/PRJ.4.000B14
- Dasgupta R, Ahlawat S, Verma RS, Gupta PK. Optical orientation and rotation of trapped red blood cells with Laguerre-Gaussian mode. *Opt Express* (2011) 19:7680. doi:10.1364/OE.19.007680
- Toyoda K, Takahashi F, Takizawa S, Tokizane Y, Miyamoto K, Morita R, et al. Transfer of light helicity to nanostructures. *Phys Rev Lett* (2013) 110:143603. doi:10.1103/PhysRevLett.110.143603
- Lin D, Daniel JMO, Clarkson WA. Controlling the handedness of directly excited Laguerre-Gaussian modes in a solid-state laser. *Opt Lett* (2014) 39:3903. doi:10.1364/OL.39.003903
- Cao X, Liu Y, Xian A, Li Y, Wu K, Xu X, et al. Direct generation of ultrafast vortex beam from a Tm:CaYAlO₄ oscillator featuring pattern matching of a folded-cavity resonator. *Opt Express* (2021) 29:39312. doi:10.1364/OE.437584
- Liu Q, Zhao Y, Zhou W, Zhang J, Wang L, Yao W, et al. Control of vortex helicity with a quarter-wave plate in an Er:YAG ceramic solid state laser. *IEEE Photon J* (2017) 9: 1–8. doi:10.1109/JPHOT.2016.2644965
- Liu Q, Zhang B, Qi S, Li Y, Fan X, Zhao Y, et al. Integration of helicity-control and pulse-modulation for vortex laser based on a black phosphorus plate. *Opt Express* (2016) 24:30031. doi:10.1364/OE.24.030031
- Zhao Y, Liu Q, Zhou W, Shen D. ~1 mJ pulsed vortex laser at 1645 nm with well-defined helicity. *Opt Express* (2016) 24:15596. doi:10.1364/OE.24.015596
- He H-S, Chen Z, Li H-B, Dong J. Low-threshold, nanosecond, high-repetition-rate vortex pulses with controllable helicity generated in Cr,Nd:YAG self-Q-switched microchip laser. *Laser Phys* (2018) 28:055802. doi:10.1088/1555-6611/aaad4c
- Khonina SN, Kotlyar VV, Shinkaryev MV, Soifer VA, Uspleniev GV. The phase rotor filter. *J Mod Opt* (1992) 39:1147–54. doi:10.1080/09500349214551151
- Kotlyar V, Kovalev A, Porfirev A, Kozlova E. Orbital angular momentum of a laser beam behind an off-axis spiral phase plate. *Opt Lett* (2019) 44:3673–6. doi:10.1364/OL.44.003673
- Khonina SN, Podlipnov VV, Karpeev SV, Ustinov AV, Volotovskiy SG, Ganchevskaya SV. Spectral control of the orbital angular momentum of a laser beam based on 3D properties of spiral phase plates fabricated for an infrared wavelength. *Opt Express* (2020) 28:18407–17. doi:10.1364/OE.396199
- Semmler M, Berg-Johansen S, Chille V, Gabriel C, Banzer P, Aiello A, et al. Single-mode squeezing in arbitrary spatial modes. *Opt Express* (2016) 24:7633. doi:10.1364/OE.24.007633
- Li R, Ren Y, Liu T, Wang C, Liu Z, Zhao J, et al. Generating large topological charge Laguerre-Gaussian beam based on 4K phase-only spatial light modulator. *Chin Opt Lett* (2022) 20:120501. doi:10.3788/COL202220.120501
- Ando T, Ohtake Y, Matsumoto N, Inoue T, Fukuchi N. Mode purities of Laguerre-Gaussian beams generated via complex-amplitude modulation using phase-only spatial light modulators. *Opt Lett* (2009) 34:34–6. doi:10.1364/OL.34.000034
- Ren Y-X, Li M, Huang K, Wu J-G, Gao H-F, Wang Z-Q, et al. Experimental generation of Laguerre-Gaussian beam using digital micromirror device. *Appl Opt* (2010) 49:1838. doi:10.1364/AO.49.001838
- Chen Y, Fang Z-X, Ren Y-X, Gong L, Lu R-D. Generation and characterization of a perfect vortex beam with a large topological charge through a digital micromirror device. *Appl Opt* (2015) 54:8030–5. doi:10.1364/AO.54.008030
- Abramochkin E, Volostnikov V. Beam transformations and nontransformed beams. *Opt Commun* (1991) 83:123–35. doi:10.1016/0030-4018(91)90534-K
- Beijersbergen MW, Allen L, van der Veen HELO, Woerdman JP. Astigmatic laser mode converters and transfer of orbital angular momentum. *Opt Commun* (1993) 96: 123–32. doi:10.1016/0030-4018(93)90535-D
- Wang D, Wang D, Wang D, Lei M, Lin S, Lin S, et al. Generation of a mode-tunable optical vortex based on a mirror curvature dynamically controlled Z-shaped resonant cavity. *Opt Lett* (2021) 46:3079–82. doi:10.1364/OL.422316
- Shen Y, Meng Y, Fu X, Gong M. Wavelength-tunable Hermite-Gaussian modes and an orbital-angular-momentum-tunable vortex beam in a dual-off-axis pumped Yb:CALGO laser. *Opt Lett* (2018) 43:291. doi:10.1364/OL.43.000291
- Zheng Y, Lei M, Lin S, Wang D, Xue Q, Huang L. Filtered influence function of deformable mirror for wavefront correction in laser systems. *Photonics* (2021) 8:410. doi:10.3390/photonics8100410
- Lin S, Wang D, Kang S, Zheng Y, Huang L. Theoretical and experimental research on the mode modulation regulation for the mode-tunable vortex laser based on mode conversion and intra-cavity modulation. *Photonics* (2022) 9:232. doi:10.3390/photonics9040232